Materials Science & Engineering A 943 (2025) 148745

Contents lists available at ScienceDirect

Materials Science & Engineering A

journal homepage: www.elsevier.com/locate/msea

Modelling the creep behaviour of Waspaloy under varying stresses and temperatures using the 6-θ methodology

Mark Evans [a,*], Mark Whittaker [a], William Harrison [b]

[a] Institute of Structural Materials, Swansea University Bay Campus, SA1 8EN, Swansea, Wales, UK
[b] Department of Science and Engineering Swansea University Bay Campus, SA1 8EN, Swansea, Wales, UK

ARTICLE INFO

Keywords:
Waspaloy
Creep
Superalloy
Hardening rules
6-θ
Methodology
Internal variables

ABSTRACT

In this paper an internal variables approach, set within a 6-θ methodology, is used to predict the strain rates associated with Waspaloy specimens tested under uniaxial but varying test conditions. The experimental results obtained for a simple loading and offloading cycle showed that predictions from such an approach were better than those obtained with a 4-θ methodology. It was also shown that the stochastic nature of creep meant that reliable predictions under variable test conditions required the use of data from repeat testing at constant test conditions. The results obtained from tests with varying but positive stresses and temperatures, showed much better strain rate predictions compared to standard time and strain hardening techniques. It also produced better predictions compared to the implementation of the internal variable approach within the 4-θ methodology.

1. Introduction

Most of the large, publicly available creep data bases [1–3], are made up of results obtained from uniaxial creep tests that have taken place under either constant load or stress and at constant temperature. Within the aerospace sector, the understanding and prediction of creep strains for materials used in high-temperature applications, such as Nickel-based super alloys, is particularly important to prevent blades rubbing against the outer casing of an aeroengine. But typically, the components within aero engines, such as turbine blades, experience cyclical variations in both stress and temperature during operational service. There is therefore great importance attached to understanding how the results contained within these creep data bases can be used to model creep during real operational service. Such an understanding is also important for constructing numerical models of creep deformation. For example, the small punch test offers the potential for understanding creep behaviour using much less material than conventional uniaxial testing. But within this test the stresses are continually changing and so there is a need to integrate this phenomenon with the readily available constant stress creep data.

Harrison et al. [4]. have published results from creep tests where the stress, temperature or both are varied during a uniaxial test. The material they used was Waspaloy. Complex conditions were studied in which both the stress and temperature were changed and the lengths of time between such changes were also varied. For example, Fig. 1 reproduces their results obtained from a repetition of 24 h of testing at 873K/880 MPa followed by 24 h of testing at 1023K/390 MPa until failure is observed. The starting point to modelling this type of data is an expression to describe a uniaxial creep curve at constant stress and temperature. These authors used the 4-θ methodology [5] that uses following equation

$$\varepsilon = \theta_1\left(1 - e^{-\theta_2 t}\right) + \theta_3\left(e^{\theta_4 t} - 1\right) \tag{1a}$$

where ε is uniaxial strain, t is time and the θ_i are parameters dependent on stress and temperature. To move from explaining the shape of a creep curve at constant stress and temperature to one derived under changing test conditions, requires identifying the starting point on a new creep curve associated with a changed test condition, i.e. a method for hardening needs to be specified. Under time hardening, the point on the new creep curve is taken to be that associated with the time at which the test condition changed. Under strain hardening, the point on the new creep curve is taken to be that associated with the strain already accumulated at the time at which the test condition changed. Life-fraction hardening calculates the point on the new curve based on the effective time which is equal to the time at which the test condition changes (t), divided by rupture time (t_f) associated with the new test condition.

An alternative method of creep hardening is to base the creep rate on the applied conditions and various material state variables

* Corresponding author.
E-mail addresses: m.evans@swansea.ac.uk (M. Evans), m.t.whittaker@swansea.ac.uk (M. Whittaker), w.harrison@swansea.ac.uk (W. Harrison).

https://doi.org/10.1016/j.msea.2025.148745
Received 19 February 2025; Received in revised form 23 June 2025; Accepted 30 June 2025
Available online 1 July 2025

$$\dot{\varepsilon} = \Phi\left(\sigma, T, \xi_1, \xi_2, \ldots, \xi_\alpha, \ldots, \xi_p\right) \quad (1b)$$

where T is temperature, σ is stress and ξ_α ($\alpha = 1, p$) are internal material state variables each dependent on the loading history of the material. All the ξ_α describe continuum quantities that could be classified as either hardening or softening, static or dynamic, transitory or permanent. Using all these different methods of hardening, Harrison et al. [4]. proceeded to predict the strain rate data seen in Fig. 1 (shown by the grey data points). However, all these approaches showed limitations in predicting the cyclical strain patterns - with the internal state variable approach performing best. Whilst this latter approach worked well for the first cycle, there was after that a tendency for the approach to under-estimate the strain rate in each cycle and to not pick up the rapid decline in strain rates at the start of each cycle. During the high temperature cycle, the method also predicted increasing strain rates with time when actual strain rates were falling or constant. The authors concluded that whilst the internal variable approach resulted in better strain rate predictions under variable test conditions, there was still room for improvement.

This paper takes a step in that direction by making use of some of the more recent modifications and advancements made to the 4-θ methodology to predict strains under changing test conditions. To achieve this aim, the paper is structured as follows. The next section outlines some of Harrison et al. [4] experimental data in more detail, together with a summary of their interpretation of this data. The methodology section reviews past approach to creep curve prediction and then outlines a theoretical underpinning of one of these approaches - the 6-θ model to be used in this paper. This section also provides a short description on how the models unknown parameters can be estimated. Results are then presented and in the conclusion section, suggestions for future research are given.

2. The data

2.1. Constant test conditions

Constant and non-constant stress creep tests were conducted by Harrison et al. [4] on the wrought Nickel based superalloy Waspaloy. The test material, supplied in bar form by Rolls Royce, had a chemical composition within the limits for Waspaloy - 18–21Cr, 12–15Co, 3.5–5Mo, 2.75–3.25Ti, 1.2–1.6Al, 0.02–0.1C and 0.003–0.01B, balance Ni (wt.%). All test specimens were solution treated at 1315 K (4 h), stabilised at 1115 K (4 h) and aged at 1030 K (16 h), with the samples air cooled between each heat treatment stage. The tests were carried out using Andrade-Chalmers constant stress cam creep machines. The test specimens were machined from the as received Waspaloy bar with the resulting cylindrical specimens having a gauge length of 22 mm and a diameter of 5 mm. These specimens were tested at the ISM (Institute of Structural Materials) and IRC (Interdisciplinary Research Centre) laboratories at Swansea University.

For the constant stress tests, five different stress-temperature test conditions were used – 823K at 1050 MPa, 873K at 880 MPa, 923K at 690 MPa, 973K at 540 MPa and 1023K at 390 MPa. At 923K the test was also replicated. The creep curves obtained at these conditions are shown in Fig. 2. The creep curves obtained at the lower temperatures (e.g. at 823K) also correspond to stresses more than the yield stress and a substantial amount of primary creep strain can be seen in these curves - the result of dislocations being continually generated under the high stress. At higher temperatures and lower stresses, creep deformation occurs under stresses below the yield stress, and deformation is accommodated by the movement of pre-existing dislocations subject to processes such as climb and cross slip - with most deformation accommodated in the grain

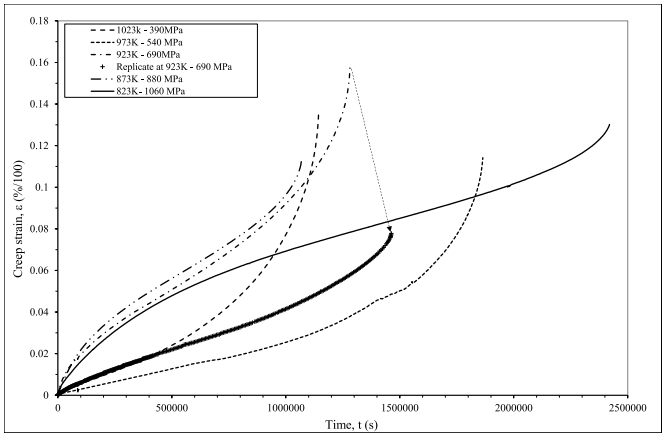

Fig. 2. Uniaxial creep curves obtained at different constant stresses/temperature conditions.

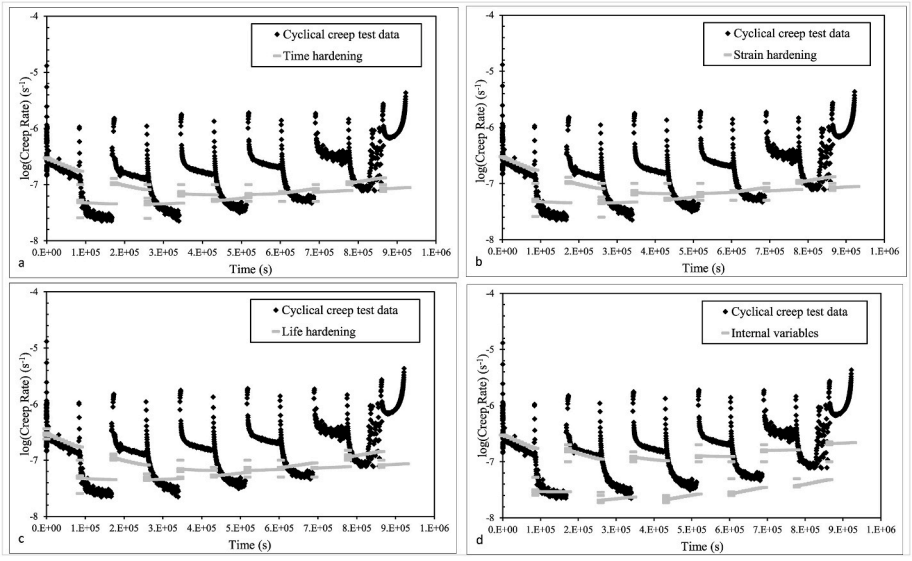

Fig. 1. Experimentally obtained creep rates from a uniaxial creep test with temperature/stress changing between 873K/880 MPa and 1023K/390 MPa every 24 h together with predicted rates obtained by Harrison et al. [4]. using a. time hardening, b. strain hardening, c. life hardening and d. internal state variable evolution within the 4-θ methodology.

boundary zones. This results in a reduced primary stage but an extended period of tertiary creep. The repeat test at 923K reveals that creep rates and lives are highly stochastic in nature.

2.2. Variable test conditions

Tensile creep tests with non-constant stress and temperature were also conducted by Harrison et al. [4]. The simplest non-constant test undertaken by these authors took the form of simple cyclical unloading. The results of this test have not been published or analysed before. Here, the test condition 923K at 690 MPa was held for a period of around 3 days, followed by unloading at this temperature for a similar period. This cycle was repeated, but after this second cycle the stress was re-applied until failure. As the temperature was kept constant throughout these cycles, there is the possibility of continued softening during the periods of off-load. Fig. 3 shows the results obtained for this simple loading and unloading experiment. In this figure (and all other figures containing the strain rate) the strain rate $\dot{\varepsilon}$ is approximated using

$$\dot{\varepsilon}_i = \left\{ \frac{9\sum_{i=-4}^{4} \varepsilon_i t_i - \sum_{i=-4}^{4}\varepsilon_i \sum_{i=-4}^{4} t_i}{9\sum_{i=-4}^{4} t_i^2 - \sum_{i=-4}^{4}(t_i)^2} \right\} \quad (1c)$$

where the subscript on t and ε denotes to the ith measurement made for time and strain respectively. Thus, the creep rate at time t_i is found by collecting the pairing $t_i\varepsilon_i$, the four $t_i\varepsilon_i$ pairings immediately below $t_0\varepsilon_0$ and the four $t_i\varepsilon_i$ pairings immediately above $t_0\varepsilon_0$ and putting a least squares linear line fit through these 9 data points. $\dot{\varepsilon}_i$ is therefore the slope of this best fit line through these 9 strain strain-time pairings.

At the start of each loading cycle there is a short period of rapid creep strain, followed by an extended period of almost constant strain rate and well-defined tertiary creep is not observed until the final period of loading. At the start of the two periods of off-loading the strain rate becomes briefly negative until a constantcreep strain rate occurs - suggesting the presence of some form of recovery.

The implications of the stochastic variability seen in Fig. 2 at 923K is again illustrated in Fig. 4. The strain rates associated with the test that has periods of off-load are in between the two tests carried out at the same conditions with no periods of off-load. Thus, the predictions of the strain rates associated with the periods of loading using the results from the constant test condition tests are likely going to be substantially overestimated using the first of the replicates. Hence it is important to present results from various replicates when making comparisons of models to obtain a feel for the natural stochastic variability, i.e. to ensure that any differences observed between actual and predicted strain rates are due to stochastic variability rather than systematic error.

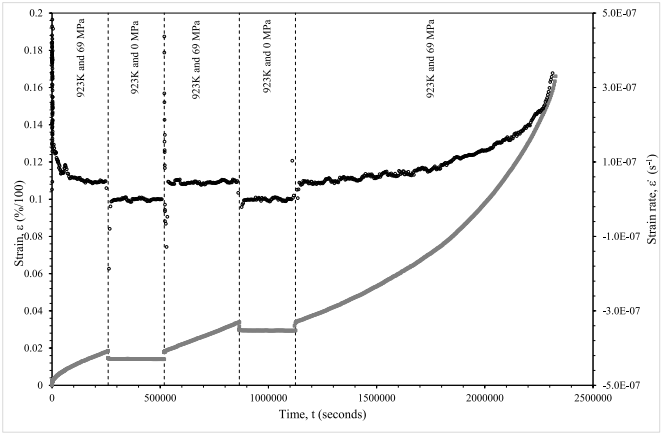

Fig. 3. Measured strain (left hand axis and grey squares) and strain rates (right hand axis and black circles) obtained under cyclical loading and unloading at 923K using 690 MPa during the loading periods and 923K - 0 MPa during the off-load periods.

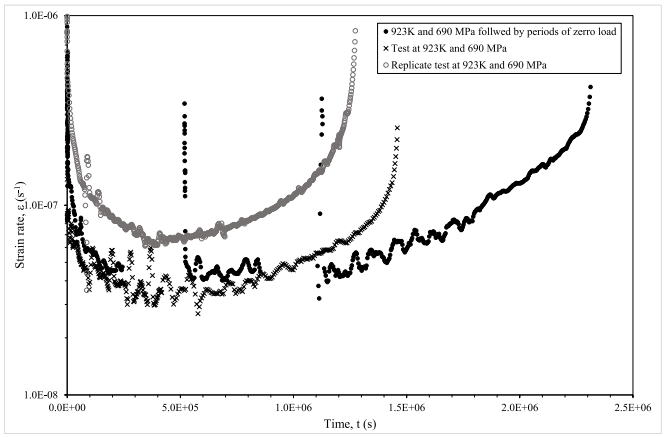

Fig. 4. Measured strain rates during the loaded periods of the cyclical loading and unloading test at 923K and 690 MPa, together with the strain rates from the replicated tests at constant 923K and 690 MPa.

The authors also conducted several tests in which the stress and temperature were changed on a cyclical basis – either every 24 h or 120 h. In this paper, analysis is confined to one of these pairings, namely 873K - 880 MPa to 1023K - 390 MPa every 24 h. A transition period of 1 h was used to allow the temperature to stabilise to each new level. During this transitionary period the stress was held at the lower of the old and new values to avoid excessive creep damage during this period. Fig. 5 shows some of the constant stress creep curves alongside those obtained under variable conditions - namely when changes from 873K to 880 MPa and 1023K - 390 MPa occur every 24 h. Up to around 400,000s the variable creep curve is in between the two constant test condition curves, but beyond that time the strains associated with the variable test are much larger than those associated with the constant stress curves.

Fig. 6 shows the creep rates associated with all the creep curves shown in Fig. 5. When test conditions were changed during a test, the initial creep rates immediately after the application of a new condition were faster than expected based on constant stress data at those conditions. This could be attributed to dislocations moving through a dislocation network forming at different applied conditions. Furthermore, at high stresses, dislocations overcome γ′ particles by cutting, whereas at low stresses dislocations overcome γ′ by diffusion-controlled climb [6]. Therefore, dislocations held up by γ' at a low stress may be freed by cutting with an increase in stress and those restricted at high stress may become mobile due to climb with an increase in temperature thus

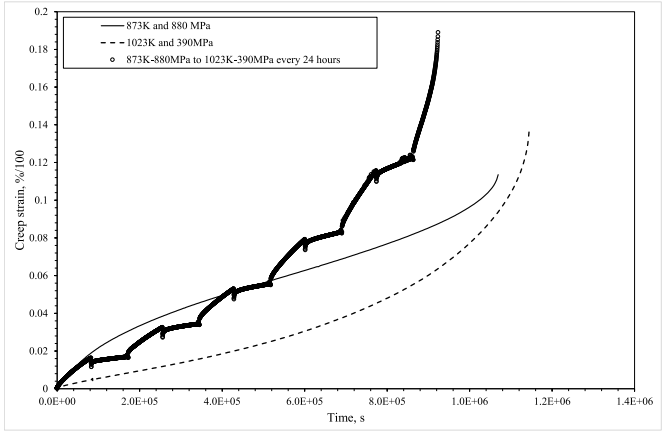

Fig. 5. Creep strains obtained from uniaxial creep tests with constant and varying test conditions.

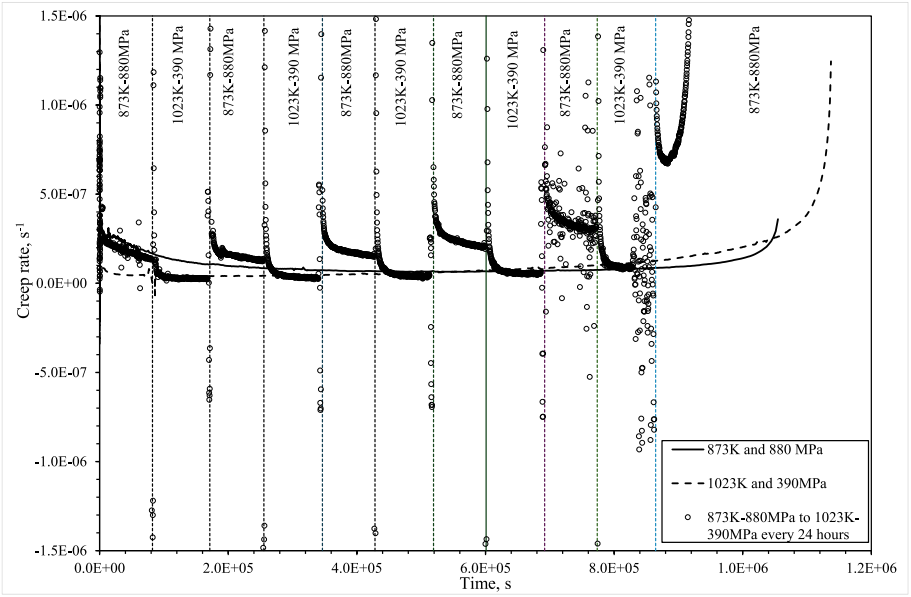

Fig. 6. Creep strain rates obtained from uniaxial creep tests with constant and varying test conditions (where the latter has temperature/stress changing from 873K/880 MPa to 1023K/390 MPa every day).

increasing the creep rate immediately following a stress and/or temperature change. Alternatively, the large primary strain rates could be due to grain boundary sliding in very early primary creep. Parkin and Birosca [7] identified a significant role for grain boundary sliding in the deformation of Waspaloy using EBSD. They found that the effective obstacle to slip transfer remained carbide presence on the grain boundary between the grains. In fact, the distortion of the areas in the vicinity of carbide rich grain boundaries could inhibit the slip continuity and caused slip direction diversion. Whatever the exact cause, these initial high creep rates rapidly decrease, and for a short period become negative when the test condition is changed.

3. Methodology

3.1. Uniaxial creep under unchanging test conditions

The literature is rich with empirical equations that can and have been used to account for the shape of a uniaxial creep curve obtained under constant stress (or load) and temperature. Many of the more recent approaches are made up of components contained within the classical representations of primary, secondary and tertiary creep deformation. Thus, Graham and Walles [8], McVetty [9] and Phillips [10] put forward a power law, exponential and logarithmic equation respectively to describe primary creep, whilst McHenry [11], Rabotnow-Kachanov [12,13] and Sandströmg-Kondyr [14] put forward exponential based equations to describe tertiary creep. Norton [15] used a power law equation to describe secondary creep. Othman and Hayhurst [16] extended the Rabotnow – Kachanov model to incorporate primary creep, whilst Maruyama et al. [17] extended the Phillips model to also include tertiary creep. Wu et al. [18], in their study of Waspaloy, developed a true stress model to explain tertiary creep, and combined this with a model of grain boundary sliding for primary creep, resulting in

$$\varepsilon = \varepsilon_p \left(1 - e^{-\frac{t}{t_p}}\right) + \frac{1}{M}\left(e^{Mkt} - 1\right) \tag{2}$$

where ε_p is strain at the end of the primary stage of creep and t_p the time at which this stage is completed, and M and k are additional model parameters. The authors stress that other models, that relate to different creep mechanisms can be added to their model, so their model does require a pre-specification of the exact creep mechanisms taking place during the primary stages.

The Theta Projection Methodology [5] can be viewed as an extension of the exponential model put forward by McVetty to pick up tertiary creep

$$\varepsilon = \theta_1\left(1 - e^{-\theta_2 t}\right) + \theta_3\left(e^{\theta_4 t} - 1\right) \text{ with } \theta_l = e^{a_l + b_l\sigma + c_l T + d_l \sigma T} \; l = 1 \text{ to } 4 \tag{3}$$

where $a_l - d_l$ are model parameters, σ is stress and T is temperature. This 4-θ methodology has the same form as Equation (2), but the parameters have very different interpretations, but both imply a minimum rather than a secondary creep rate. Holdsworth et al. [19], modified Equation (3) to allow for extended periods of secondary creep

$$\varepsilon = \theta_1\left(1 - e^{-\theta_2 t}\right) + \theta_3\left(e^{\theta_4 t} - 1\right) + \dot{\varepsilon}_s t \tag{4a}$$

where $\dot{\varepsilon}_s$ is the constant secondary creep rate given by $\dot{\varepsilon}_s = a\sigma^b e^{-c/RT}$ (a, b,c, are model parameters and R the universal gas constant). Liu et al. [20]. in their application to P92 steel, extended the 4-θ methodology to model creep curves derived under constant load conditions

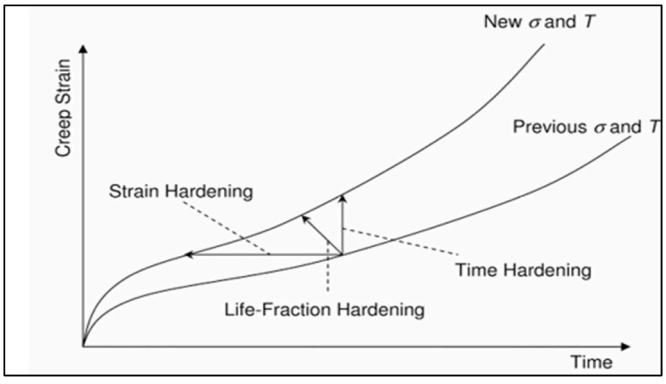

Fig. 7. Schematic representation of strain hardening, time hardening and life fraction hardening during a change in creep testing conditions.

$$\varepsilon = \theta_1\left(1 - e^{\theta_2\left[1-\frac{\sigma_o}{\sigma_Y}(1-e)\right]t}\right) + \theta_3\left(e^{\theta_4 t} - 1\right) \tag{4b}$$

where σ_Y is the yield stress and σ_o the initial and constant load. In their application to alloy 690, Moon et al. [21] used the following expression for constant load testing

$$\varepsilon = \theta_1\left(1 - e^{\theta_2 t}\right) + \theta_3\left(e^{\theta_4 t^{\theta_5}} - 1\right) \tag{4c}$$

For constant stress testing they suggested using Equation (3) but with the modification

$$\theta_l = e^{a_l + b_l\sigma_o + c_l T + d_l\sigma_o T}\ l = 1, 3 \text{ and } \theta_l = e^{a_l + b_l\sigma + c_l T + d_l\sigma T}\ l = 2, 4 \tag{4d}$$

Harrison et al. [22] used.

$$\theta_j = a_j\left(\frac{\sigma}{\sigma_{TS}}\right)^{b_j}\ j = 1, 3 \text{ and } \theta_j = a_j\left(\frac{\sigma}{\sigma_{TS}}\right)^{b_j} e^{\frac{-Q_j^c}{RT}}\ j = 2, 4 \tag{4e}$$

when studying the titanium aluminide alloy Ti-45Al-2Mn-2Nb - where σ_{TS} is the tensile strength of the material and Q_j^c the activation energy for each rate parameter. Zheng et al. [23]. considered the following three parameter simplification

$$d = \theta_1\left(1 - e^{\theta_2 t}\right) + \theta_3\left(e^{\theta_2 t} - 1\right) \tag{4f}$$

in their application to small punch test results in 1Cr-5Mo steel. The parameter d is the displacement measured during such a test and each θ parameter was made a function of the punch force.

A final example of a modification of the 4-θ methodology, often referred to as the 6-θ methodology - is that proposed by Evans [24,25].

$$\varepsilon = \theta_1\left(1 - e^{-\theta_2 t}\right) + \theta_3\left(e^{\theta_4 t} - 1\right) + \theta_5\left(1 - e^{-\theta_6 t}\right) \text{ with } \theta_l = e^{a_l + b_l\sigma + c_l T + d_l\sigma T}\ l = 1 \text{ to } 6 \tag{5a}$$

Evans [24] found that for the very ductile commercial aluminium alloy 2419, the term $\theta_1\left(1 - e^{-\theta_2 t}\right)$ was insufficient to pick up the presence of very early and strongly pronounced primary creep and so suggested adding the additional term $\theta_5\left(1 - e^{-\theta_6 t}\right)$ to account for this. Indeed, depending on the material being studied, he suggested the fully general functional form for modelling uniaxial creep at constant test conditions

$$\varepsilon = \sum_{l=1}^{q} \theta_{2l-1}\left[1 - e^{-\theta_{2l} t}\right] \tag{5b}$$

If $\theta_{2l-1} > 0$ and $\theta_{2l} > 0$ the l^{th} term in the series represent a primary process with the creep rate decreasing with increasing time. If $\theta_{2l-1} < 0$ and $\theta_{2l} < 0$ the lth term in the series represent a tertiary process with the creep rate increasing with increasing time. Theoretically, there is no limit to the value of q, but the practicalities of estimating the θ value increase dramatically with increasing q. An important advantage of the 4-θ model and its modifications is that preexisting damage can be measured directly from the θ parameters and this make the approach particularly useful for numerical models of the small punch test and other high temperature applications where the stress changes.

More importantly, each term in Equation (5b) is capable of theoretical explanations in terms of micro mechanisms governing creep. Loosely following the approach taken by Evans [26], internal state variables can be used to explain the form of Equation (3) using as a starting point the following functional for Φ in Equation (1b)

$$\dot{\varepsilon} = \dot{\varepsilon}_o f(\xi_\alpha) \tag{6a}$$

where $\dot{\varepsilon}_o$ is the initial rate of strain occurring for virgin material when placed on test - which depends on both stress and temperature. So, $f(\xi_\alpha)$ takes on the value one for such material, but thereafter is modified by the creep processes occurring within the grains and/or grain boundaries. Next assume that $f(\xi_\alpha)$ is a linear function of several of these internal variables

$$\dot{\varepsilon} = \dot{\varepsilon}_o\left\{1 + (h_1, h_2, \ldots, h_\alpha, \ldots, h_n) + (r_1, r_2, \ldots, r_\alpha, \ldots, r_m) + \left(w_1, w_2, \ldots, w_\alpha, \ldots, w_p\right)\right\} \tag{6b}$$

where h_α, r_α, and w_α are dislocation hardening, dislocation softening and damage internal variables respectively. Softening (or recovery) variables are those associated with climb and glide and are static but positive variables. On the other hand, hardening variables are dynamic in nature and will be negative in quantity. The damage variables include changes in precipitate morphology, alteration in second-phase interfaces, changes in mobile dislocation density and grain boundary cavitation and cracking – to name a few. They are usually dynamic in nature and positive in quantity. More than one process can occur at a time and each mechanism will be a function of stress and temperature.

More specially, and in relation to Waspaloy, Whittaker et al. [6]. concluded that at test conditions below the yield stress the main resistance to dislocation motion (some of the h_α hardening variables) is the interaction with the tertiary γ' precipitates. Dislocation motion is therefore limited by the climb of these dislocations over and/or around all but the smallest tertiary precipitates (some of the r_α softening variables). Above the yield stress there is a higher mobile dislocation density, and eventually the density becomes so high that dislocations become locked in tangles (some of the h_α hardening variables). Above yield, the stress is sufficient for the dislocations to cut through the tertiary precipitates (again some of the r_α softening variables). Parkin and Birosca [7] found that grain boundary sliding (some of the r_α softening variables) was a prominent source of strain accumulation in Waspaloy and that carbide rich boundaries (some of the h_α) play a considerable role in hardening.

The power of this modelling framework therefore is that it can encapsulate a large variety of different creep mechanisms without formally having to specify their exact nature. For example, it can model a situation where creep processes are dominant at different locations and at different times. Evans [25], for example, found evidence (in the form of differing activations for the theta rate parameters) in aluminium alloy 2419, that very early on in a creep test, creep processes are confined to the grain boundaries in the form of viscoelastic deformation. Then as time progresses, but still within the primary stage of creep, the dominant creep processes occur within the grains for this material all of which are dependent on hardening and softening mechanisms. Finally, damage mechanisms governed tertiary creep. If such time – location interactions are also present within Waspaloy, the framework given by

Equation (6b) is designed to model it.

3.2. Uniaxial creep under changing test conditions

The key to accurate strain rate predictions under changing test conditions, is the accurate quantification of prior hardening, softening and damage. To move from explaining the shape of a creep curve at constant stress and temperature to one derived under changing test conditions, requires a definition of hardening. Time, strain and life-fraction based hardening methods are often used to quantify the effects of prior creep on future strain rates, and these are illustrated in Fig. 7. In this figure, the test conditions are initially set at the "Previous" values for σ and T and then strain progresses along the lower creep curve seen in this figure. Then at some future point in time the test conditions are changed to "New" σ and T. Consequently, creep will then progress along the upper creep curve.

But the crucial question is from what point on this new creep curve does strain start accumulating again? Under the concept of time hardening, the point on the new creep curve is taken to be that associated with the time at which the test condition changed. This method is not suitable when there are large changes in the applied stress. Under the strain hardening concept, the point on the new creep curve is taken to be that associated with the strain already accumulated at the time at which the test condition changed. However, this method can produce inaccuracies if the conditions vary from those displaying a primary dominated creep curve to those displaying a tertiary dominated creep curve and vice versa. Life-fraction hardening attempts to address these limitations by calculating the point on the new curve based on the effective time which is equal to the time at which the test condition changes (t), divided by rupture time (t_f) associated with the new test condition. This method has the advantage of predicting creep rupture when t/t_f equals 1.

An alternative to these hardening rules is the internal variable approach given by Equation (6b). Evans [26] stated some constitutive creep equations that lead-to the 4-θ equation – Equation (1a). As the internal variables in Equation (6b) occur linearly, and because Equation (6b) is linear in the coefficients, it is possible to quantify over-all hardening (H), softening (R) and damage (W) through a simple summation

$$H=\sum_{\alpha=1}^{n} h_\alpha \; ; \; R=\sum_{\alpha=1}^{m} r_\alpha \text{ and } W=\sum_{\alpha=1}^{p} w_\alpha \tag{7a}$$

Evans then postulated the following evolutionary equations for these internal variables

$$\dot{H}=-\widehat{H}\dot{\varepsilon} \; ; \; \dot{R}=\widehat{R} \text{ and } \dot{W}=\widehat{W}\dot{\varepsilon} \tag{7b}$$

where the dot above each variable refers to the rate of change in this variable with respect to time and $\widehat{H}$, $\widehat{R}$ and $\widehat{W}$ are parameter constants found as

$$\widehat{H}=\sum_{\alpha=1}^{n} \widehat{h}_\alpha \; ; \; \widehat{R}=\sum_{\alpha=1}^{m} \widehat{r}_\alpha \text{ and } \widehat{W}=\sum_{\alpha=1}^{p} \widehat{w}_\alpha \tag{7c}$$

where $\dot{h}_\alpha = -\widehat{h}_\alpha\dot{\varepsilon}$, $\dot{w}_\alpha=\widehat{w}_\alpha\dot{\varepsilon}$ and $\dot{r}_\alpha=\widehat{r}_\alpha$. Equation (6b) can then be written as

$$\dot{\varepsilon}=\dot{\varepsilon}_o(1+H+R+W) \tag{7d}$$

Under the assumption that primary creep occurs over small times in relation to the creep life, Evans [26] has shown that Equations (7) lead to

$$\dot{\varepsilon}=\left[\dot{\varepsilon}_o-\frac{\widehat{R}}{\widehat{H}}\right]e^{-\widehat{H}\dot{\varepsilon}_o t}+\frac{\widehat{R}}{\widehat{H}}e^{\frac{\widehat{W}\widehat{R}}{H}t} \tag{8a}$$

and

$$\varepsilon=\frac{1}{\widehat{H}\dot{\varepsilon}_o}\left[\dot{\varepsilon}_o-\frac{\widehat{R}}{\widehat{H}}\right]\left(1-e^{-\widehat{H}\dot{\varepsilon}_o t}\right)+\frac{1}{\widehat{W}}\left(e^{\frac{\widehat{W}\widehat{R}}{H}t}-1\right) \tag{8b}$$

Although the condition of short-lived primary creep is met by many particle-hardened alloys, this approach does not suggest that it applies to all materials irrespective of testing conditions. Further, the assumption does not remove the appearance of damage from early primary creep - as all terms in Equation (8a) contain those parameters ($\dot{\varepsilon}_o$, $\widehat{H}$, $\widehat{R}$,$\widehat{W}$) and so control primary creep. Damage is restricted to the generation to those strains arising from the secondary process, which is also present throughout the whole of primary creep. There is some evidence to support this. The well-established Monkman-Grant relations [27] relates fracture behaviour to the product of secondary creep rate and failure time rather than total strain

Another important advantage of this theta methodology is that all the internal variables can be easily and directly calculated from the θ values describing a creep curve. So, comparing Equation (8b) to Equation (1a), it follows that

$$\dot{\varepsilon}_o=\theta_1\theta_2+\theta_3\,\theta_4;\; \widehat{W}=\frac{1}{\theta_3} \; ; \; \widehat{H}=\frac{\theta_2}{\dot{\varepsilon}_o} \; ; \; \widehat{R}=\frac{\theta_2\theta_3\theta_4}{\dot{\varepsilon}_o} \tag{8c}$$

It is easy to use Equations (8a-c) for time hardening. In the case of a test where stress and temperature change, strain rate predictions are made in the following way. For an initial stress-temperature combination the θ_l values for a constant stress test at this condition are used to calculate $\dot{\varepsilon}_o$, $\widehat{H}$, $\widehat{R}$, and $\widehat{W}$ using Equation (8c). These are then inserted into Equation (8a) to predict strain rates during this initial cycle. Then for the next cycle where a new stress-temperature combination exists, the θ_l values for the constant stress test at this condition are used to re-calculate $\dot{\varepsilon}_o$, $\widehat{H}$, $\widehat{R}$,and $\widehat{W}$. These are then re-inserted into either Equation (8a) to predict strain rates during the second cycle. This can be repeated for all the cycles making up the test data. If constant stress tests don't exist for a test condition in the variable test, then they can be estimated using

$$\ln[\theta_l]=a+b\sigma+cT+d\sigma T \; l=1 \text{ to } 4 \tag{8d}$$

where the parameters a to d require estimation. Let strain rate predictions calculated in this way be called 4-θTH. The procedure for strain hardening is similar. The θ_l values for the constant stress test conditions associated with the first cycle are inserted into Equations (8a-c) to predict strain and strain rates up to the end of the first test cycle. Let t_1 be the time associated with the end of the first cycle and ε_1 the strain predicted at this time using Equation (8b). The θ_l values for the constant stress test conditions associated with the second cycle are then inserted into Equation (8b) together with the strain value ε_1. Solving this equation for the t value that equals this inserted strain then yields a prediction for the time it would have taken to reach a strain of ε_1 under the constant stress test conditions associated with the second cycle – t*. Strain rate predictions for the second cycle are then found by inserting the θ_l values for the constant stress test conditions associated with the second cycle and time values equal to $t_i = \Delta t_i + t^*$ into Equation (8a). This process can then be repeated for all the test cycles. Let strain rate predictions calculated in this way be called 4-θSH.

The internal variable approach to hardening is different to 4-θTH, with predictions depending on what assumptions are used to simplify Equation (7d). For virgin material, H, R and W in Equation (7d) are all equal to zero, but as creep progresses their values can be updated during each experimentally recorded time increment $\Delta t_i = t_i - t_{i-1}$ in different ways depending on which assumptions are made. If it is assumed that in primary creep, there is no damage accumulation (W = 0), then it follows from Equations (7b)–(7d)

$$H_{i+1} = H_i - \widehat{H}\dot{\varepsilon}_o(1 + H_i + R_i)\Delta t_i \; ; \; R_{i+1} = R_i + \widehat{R}\Delta t_i \; ; \; W_{i+1} = W_i + \frac{\widehat{W}\widehat{R}}{\widehat{H}}(1 + W_i)\Delta t_i \tag{9a}$$

with

$$\dot{\varepsilon}_i = \dot{\varepsilon}_o\left(1 + H_i + R_i + \frac{\widehat{R}}{\dot{\varepsilon}_o\widehat{H}}W_i\right) \tag{9b}$$

for i = 1 to v, where i in an indicator for each experimental time recording, so that i = 1 is the first recorded time, i = 2 for the second and so on (where there is v such recordings in total). This iterative process is set in motion by setting $H_{i=1} = R_{i=1} = W_{i=1} = 0$. Let the strain rate predictions based on Equations (9a)–(9b) be called 4-θIV1.

To modify this analysis to account for the 6-θ specification given by Equation (5a), an extension of the above method is required. One approach is to split primary creep into two separate phases (early and latter) and allow hardening and softening to occur in both stages. Under this scenario the creep rate in the early primary stage will tend towards a constant rate $\frac{\widehat{R}_1}{\widehat{H}_1}$ where the rate parameters in this ratio refer to rates of hardening and softening exclusive to early primary creep. The role of hardening and softening in latter primary creep is then to accelerate this steady state creep rate, with the creep rate in the latter stage tending towards the steady state rate of $\frac{\widehat{R}_2}{\widehat{H}_2}$ – which is often referred to as the minimum creep rate. Damage then accelerates this minimum creep rate (where the parameters in this second ratio refer to rates of hardening and softening exclusive to latter primary creep). The Appendix to this paper contains details of how all this can be expressed as a direct function of time

$$\dot{\varepsilon} = \left[\dot{\varepsilon}_o - \frac{\widehat{R}_1}{\widehat{H}_1}\right]e^{-\widehat{H}_1\dot{\varepsilon}_o t} + \left[\dot{\rho}_{1o} - \frac{\widehat{R}_2}{\widehat{H}_2}\right]e^{-\widehat{H}_2\dot{\rho}_{1o}t} + \frac{\widehat{R}_2}{\widehat{H}_2}e^{\frac{\widehat{W}\widehat{R}_2}{\widehat{H}_2}t} \tag{10a}$$

where $\dot{\rho}_{1o} = \frac{\widehat{R}_1}{\widehat{H}_1}$. The actual creep curve is found upon the integration of Equation (10a)

$$\varepsilon = \frac{1}{\widehat{H}_1\dot{\varepsilon}_o}\left[\dot{\varepsilon}_o - \frac{\widehat{R}_1}{\widehat{H}_1}\right]\left(1 - e^{-\widehat{H}_1\dot{\varepsilon}_o t}\right) + \frac{1}{\widehat{H}_2\dot{\rho}_{1o}}\left[\dot{\rho}_{1o} - \frac{\widehat{R}_2}{\widehat{H}_2}\right]\left(1 - e^{-\widehat{H}_2\dot{\rho}_{1o}t}\right) + \frac{1}{\widehat{W}}\left(e^{\frac{\widehat{W}\widehat{R}_2}{\widehat{H}_2}t} - 1\right) \tag{10b}$$

Comparing Equation (10b) to Equation (5a), it follows that

$$\dot{\varepsilon}_o = \theta_1\theta_2 + \theta_3\theta_4 + \theta_5\theta_6; \; \dot{\rho}_{1o} = \theta_1\theta_2 + \theta_3\theta_4 \tag{11a}$$

$$\widehat{W} = \frac{1}{\theta_3} \; ; \; \widehat{H}_1 = \frac{\theta_6}{\dot{\varepsilon}_o} \; ; \; \widehat{H}_2 = \frac{\theta_2}{\dot{\rho}_{1o}} \; ; \; \widehat{R}_1 = \frac{\theta_6}{\dot{\varepsilon}_o}[\dot{\varepsilon}_o - \theta_5\theta_6] \; ; \; \widehat{R}_2 = \frac{\theta_2}{\dot{\rho}_{1o}}[\dot{\rho}_{1o} - \theta_1\theta_2] \tag{11b}$$

The internal variable approach using six theta parameters under the above assumptions takes the following form. First, it is assumed that in all primary stages of creep, there is no damage accumulation (W = 0) and the causes of hardening and softening in the two stages of primary creep are distinctly different. H_1 and R_1 accelerate the initial creep rate $\dot{\varepsilon}_o$, whilst H_2 and R_2 accelerate the steady state rate $\frac{\widehat{R}_1}{\widehat{H}_1}$. Damage is then assumed to take place during tertiary creep only. It then follows that

$$H_{1i+1} = H_{1i} - \widehat{H}_1\dot{\varepsilon}_o(1 + H_{1i} + R_{1i})\Delta t_i \; ; \quad H_{2i+1} = H_{2i} - \widehat{H}_2\frac{\widehat{R}_1}{\widehat{H}_1}(1 + H_{2i} + R_{2i})\Delta t_i \tag{12a}$$

$$R_{1i+1} = R_{1i} + \widehat{R}_1\Delta t_i \; ; \; R_{2i+1} = R_{2i} + \widehat{R}_2\Delta t_i : W_{i+1} = W_i + \widehat{W}\frac{\widehat{R}_2}{\widehat{H}_2}(1 + W_i)\Delta t_i \tag{12b}$$

with

$$\dot{\varepsilon}_i = \dot{\varepsilon}_o\left(1 + H_{1i} + R_{1i} + \frac{\widehat{R}_1}{\dot{\varepsilon}_o\widehat{H}_1}[H_{2i} + R_{2i}] + \frac{\widehat{R}_2}{\dot{\varepsilon}_o\widehat{H}_2}W_i\right) \tag{12c}$$

This iterative process is set in motion by setting $H_{1,i=1} = H_{2,i=1} = R_{1,i=1} = R_{2,i=1} = W_{i=1} = 0$. Let the strain rate predictions based on Equation (12) will be called 6-θIV1.

For a test where the stress varies between some positive value and zero, but the temperature is held fixed, a different procedure must be used as theta values are not defined for zero stress. Hence it is difficult to predict what will happen during periods of off-load using the theta methodology. With some, simplifications however, the strain rates during the loaded periods can be modelled. It is well known that when a stress is suddenly reduced in a constant stress creep test, the strain rate will change in a way that depends on the magnitude of this stress change relative to the internal stresses opposing continued forward motion of a dislocation (and each dislocation experiences a different internal stress). The difference between these two forces is termed the effective stress and for small reductions in the applied stress the effective stress will remain positive, and the creep rate will slow down but remain positive. For such situations the above approach can be used. But when the stress is reduced to zero, the effective stress will clearly be negative, forcing most dislocations to reverse direction, so that a negative creep rate will occur. However, the size of this negative strain rate cannot be determined from a constant stress test and so this paper assumes that during periods of offload, hardening (H_1 and H_2) remain equal to the value at the end of the previous loaded cycle.

It will also be assumed that when the stress is removed no further damage occurs so the value for W remains the same as the last value observed during the previous loaded cycle. The assumption that damage is not reversable is reasonable, but it must be noted that more realistically hardening will be partially or completely reversed or annihilated during the offload phase. But more experimentation is needed to see if the rate of such reversal is simply the opposite of $\widehat{H}_1$ and $\widehat{H}_2$. What happens to softening during the periods of offload are uncertain. One possibility is that it continues at rates given by $\widehat{R}_1$ and $\widehat{R}_2$. But as these softening rates depends on both stress and temperature, and only temperature is unchanged during the offload period, it is likely these rates will be a fraction of those associated with the loaded cycles. This paper will therefore look at strain rate predictions associated with softening rates being given by $\widehat{\lambda R}_1$ and $\widehat{\lambda R}_2$ during periods of offload for a few scenario values for λ between 0 and 1. Let the predictions obtained under these simplifying assumptions be termed 6-θIV2.

3.3. Estimation

Evans [28] developed a non-linear least squares procedure to estimate the θ_l values in Equation (1a) from the strain-time results obtained from a uniaxial creep test carried out at constant stress and temperature. The theta parameters are obtained by iteratively carrying out a series of linear regressions, where the variables in these regressions are a set of derivative variables. Starting values for the θ_l parameters are first chosen – $\theta_{j,0}$. This enables the residual strain series to be calculated as

$$e_{i,o} = \varepsilon_i - \left\{\theta_{1,0}\left(1 - e^{-\theta_{2,0}t_i}\right) + \theta_{3,0}\left(\theta_{4,0}e^{\theta_{4,0}t_i} - 1\right)\right\} \tag{13a}$$

These starting values can then be used to compute initial values for the analytical first derivatives

$$\frac{de_{i,0}}{d\theta_{l,0}} \text{ for } l = 1, 4 \tag{13b}$$

Table 1
Estimated θ_l for Equation (1a) and Equation (5a) obtained using the Gauss-Newton approach summarised by Equation (13).

Row		(θ_1)	(θ_2)	(θ_3)	(θ_4)	(θ_5)	(θ_6)
		6-θ					
1	880 MPa and 873K	0.03053	8.13E-06	0.04822	1.12E-06	0.00150	5.53E-04
2	690 MPa and 923K	0.04742	2.44E-06	0.00393	2.42E-06	0.00840	0.000048
3	690 MPa and 923K*	0.02702	1.761E-06	0.00331	1.87E-06	0.00109	6.67E-05
4	390 MPa and 1023K	0.00803	3.30E-06	0.00606	2.50E-06	0.00147	0.000139
		4-θ					
5	880 MPa and 873K	0.030745	8.41E-06	0.049679	8.25E-07	–	–
6	690 MPa and 923K	0.03097	7.43E-06	0.019123	1.44E-06	–	–
7	390 MPa and 1023K	0.01791	2.39E-06	0.003485	2.92E-06	–	–

*Replicate.

where for example

$$\frac{de_{i,o}}{d\theta_{2,o}} = t_i \theta_{1,0}\, e^{-\theta_{2,o} t_i} \tag{13c}$$

A first order Taylor series approximation to Equation (13a) is given by

$$e_{i,o} \cong \left(\theta_{1,1} - \theta_{1,0}\right) \frac{de_{i,o}}{d\theta_{1,o}} + \ldots\ldots\ldots + \left(\theta_{4,1} - \theta_{4,0}\right) \frac{de_{i,o}}{d\theta_{4,0}} \tag{13d}$$

and so the regression coefficients obtained from a multiple regression of $e_{i,o}$ on all the $\frac{de_{i,o}}{d\theta_{j,o}}$ will yield updated values for all the theta parameters, i.e. $\theta_{1,1}$ is an improved estimate for θ_1 (compared to the starting value $\theta_{1,o}$). $\theta_{1,1}$ to $\theta_{4,1}$ then replace $\theta_{1,0}$ to $\theta_{4,0}$ and the above steps are repeated until the updated theta estimates are the same as the previous values (or to within a pre-defined small difference). This Gauss-Newton procedure is implemented within Excel with a straightforawrd extension of this method to include six theta parameters and an account for first order autocorrelation in the $e_{i,j}$ series.

4. Results

4.1. Theta values

Table 1 shows the estimates for the θ_l (l = 1 to 6) values obtained at 390 MPa and 1023K (row 4), together with the estimated values for θ_l at 873K and 923K (rows 1 and 3). They were obtained using the non-linear least squares method described in the previous sub section. The bottom half of the table (rows 5–7) shows estimates for θ_1 to θ_4 associated with Equation (1a) – these are the same values as obtained by Harrison [4] et al.

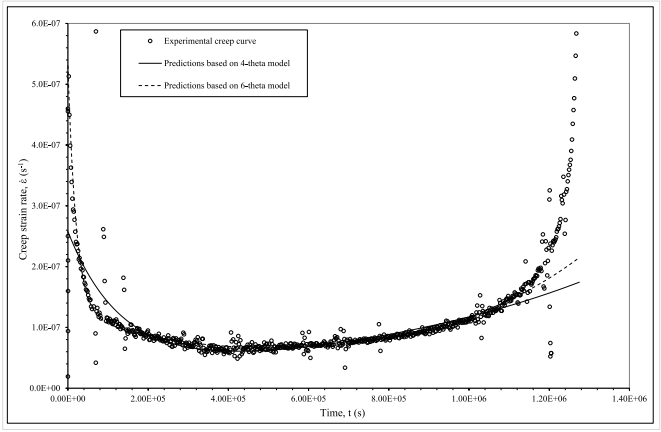

Fig. 8. Experimental creep rates obtained at 923K and 690 MPa over the full length of time to failure, together with the predictions based on the θ values in rows 2 (6-θ equation) and 6 (4-θ equation) of Table 1.

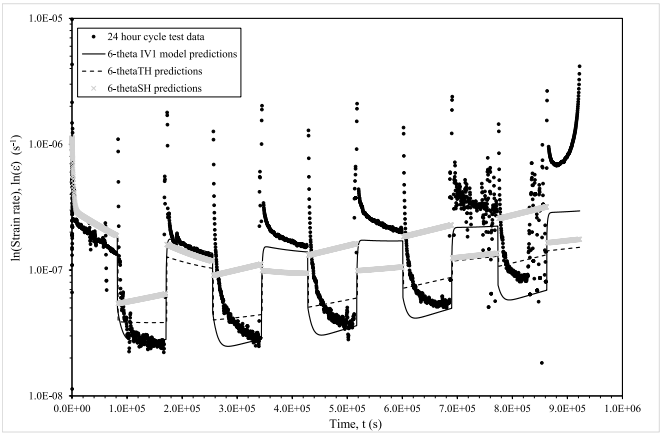

Fig. 9. Creep strain rates from testing for 24 h at 880 MPa and 873K followed by 24 h at 390 MPa and 1023K, together with predicted strain rates obtained from the 6-θTH model (dashed line), 6-θSH model (grey line) and the 6-θIV1 (solid line) models.

The fit to the experimental creep rates obtained at 923K and 690 MPa using these theta values in conjunction with Equations (1a), (5a) are shown in Fig. 8. The fit to the experimental strain rates is better for the 6-θ model over the very early stages of primary creep and the latter stages of primary creep but there is a noticeable deviation in the predictions from both equations close to the failure time. This deviation can be attributed to necking where the creep rate accelerates away from the expected exponential relationship.

4.2. 24-Hour cyclical variation in stress and temperature

The strain rates in Fig. 6 correspond to testing for 24 h at 880 MPa and 873K followed by 24 h at 390 MPa and 1023K. These two cycles are repeated until failure occurs. At the start of the first cycle the initial creep rate rapidly diminishes at first followed by a slower but constantly diminishing creep rate. Then when stress is reduced with a corresponding rise in temperature the same pattern in the strain rate is observed but with the strain rate at the end of this cycle being much lower than at the end of the first cycle. This pattern repeats itself every two cycles with a tendency for the creep rate at the end of each cycle being higher than the previous corresponding cycle. Fig. 9 plots the predictions from various 6-θ models against these experimentally derived strain rates. The black dashed line shows the predictions from the 6-θTH model – i.e. time hardening within the 6-θ methodology. During the first cycle the model predicts the initial strain rate reasonably well and the shape of the declining creep rate thereafter, albeit at a higher strain-time profile. The model then predicts the large fall in the creep rate at the very start of the next cycle but then predicts an

unchanging creep rate for the remainder of this cycle, whilst the actual creep rate continues to fall. The model then predicts most but not all of the large increase in the creep rate at the very start of the next cycle, and then underpredicts predicts the declining creep rate for the remainder of this cycle although it predicts the direction of change in the creep rate. The nature of these predictions then remains the same for the remaining cycles, with predicted damage accumulation during the high temperature cycles leading to an upward trend in the creep rate when the actual creep rate continues to decline. In the lower temperature cycles, there is an under prediction of damage accumulation leading to the degree of underprediction increasing.

The predictions from the 6-θSH model (using strain hardening) are shown by the light grey line and are worse than the those obtained using time hardening. During the second cycle the overpredictions are more pronounced compared to the 6-θTH model and more so in the wrong direction. During the third cycle the predictions are better when using the 6-θSH model, but for the remaining low temperature cycles the time hardening and strain hardening models produce similar results (and so are indistinquishable in this figure). The predictions for the remaining high temperature cycles become more and more unrealistic with time when using strain hardening.

The predictions from the 6-θIV1 model (using internal variables) are given by the solid line and are better than the those obtained using both time and strain hardening. During the second cycle this model traces out the time profile of the strain rates extremely well and it also picks up the increased strain rate at the start of the third cycle and its subsequent time profile very well. From then on, the model mimics the time profiles of the strain rates in each cycle, but tends to under predict the magnitude of the strain rate – probably due to not picking up enough damage accumulation.

Fig. 10 compares the predictions obtained 6-θIV1 with those obtained from the 4-θIV1. The predicted strain rate time profiles are similar for the two models, but from the second cycle onwards the predicted strain rates from the 6-θIV1 model are much closer to the experimentally obtained strain rates.

The rate constant $\widehat{H}_1$ changes from −448 in the low temperature/high stress regime to −565 in the higher temperature/lower stress regime so that in Fig. 11a hardening progresses at a faster rate with respect to time in the low temperature/high stress cycle. The same is true for the internal variable H_2 in Fig. 11b, with $\widehat{H}_2$ changing from −27 to −80 between the two different cycles. With $\widehat{H}_2 < \widehat{H}_1$ in each regime, the hardening mechanisms associated with H_1 account for most of the rapidly changing strain rates observed at the start of each cycle.

The rate constant $\widehat{R}_1$ changes from 0.00015 in the low temperature/high stress regime to 2.36E-05 in the higher temperature/lower stress regime so that the in Fig. 11a softening progresses at a faster rate with respect to time in the low temperature with high stress cycle. The same is not true for the internal variable R_2 in Fig. 11b, with $\widehat{R}_2$ changing little between each cycle (changing from 1.45E-06 to 1.2oE06 between the two different cycles). Thus, in the latter stages of primary creep softening progresses at a slow rate compared to hardening. These rate constants result in a minimum creep of $\frac{\widehat{R}_2}{\widehat{H}_2} = 5.4\text{E-}08\ s^{-1}$ in the low temperature/high stress regime to $\frac{\widehat{R}_2}{\widehat{H}_2} = 1.52\text{E-}08\ s^{-1}$ in the higher temperature/lower stress regime. Without the hardening and softening mechanisms associated with the latter part of primary creep the creep rate would tend $\frac{\widehat{R}_1}{\widehat{H}_1} = 3.0\text{E-}07\ s^{-1}$ in the low temperature/high stress regime before damage started to accumulate.

The rate constant $\widehat{W}$ changes from 27 in the low temperature/high stress regime to 79 in the higher temperature/lower stress regime so that the in Fig. 11b damage progresses at a faster rate with respect to time in the high temperature/low stress cycle regime. This figure also reveals that damage does not start to accelerate until around 2E-05 s into the test – or about 25 % into the cyclical test.

Many different interpretations can be placed on these variables that would require further microstructural analysis that would be a valuable source of future research. Some interesting hypotheses that could be studied include the possibility that H_1 represents hardening in the early stages of primary creep with this hardening being confined to grain boundaries within the material and that H_2 then represents hardening taking place within the grains. The fact that H_1 evolves at a faster rate

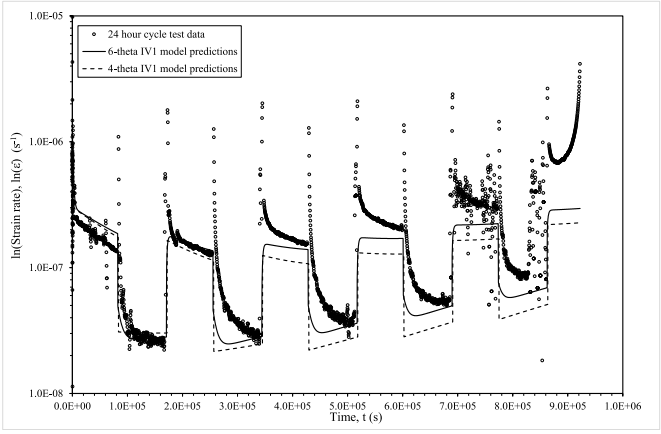

Fig. 10. Creep strain rates from testing for 24 h at 880 MPa and 873K followed by 24 h at 390 MPa and 1023K, together with predicted strain rates obtained from the 6-θTV1 model (solid line) and the 4-θTV1 model.

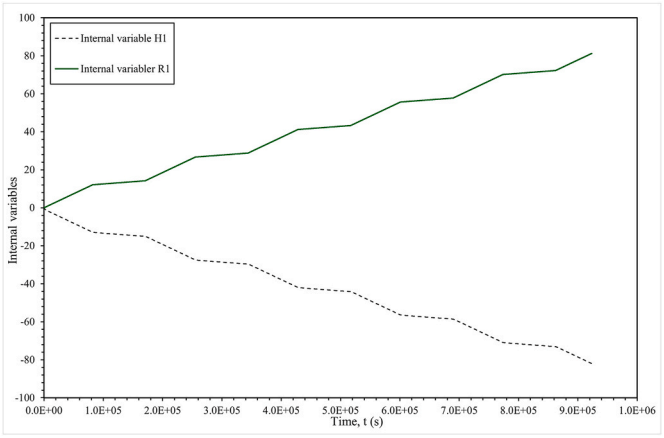

Fig. 11a. Variation of the internal variables H_1 and R_1 with time.

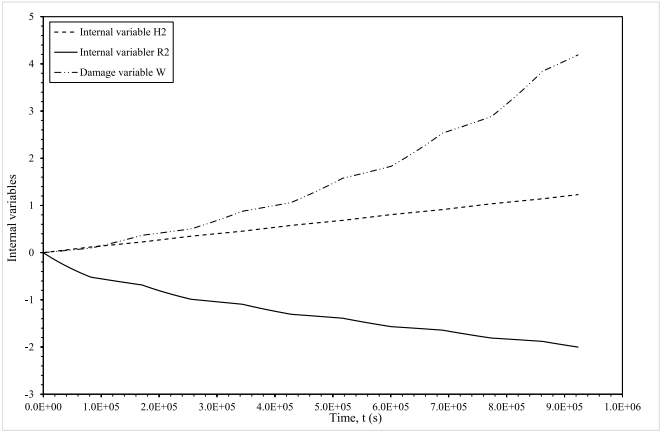

Fig. 11b. Variation of the internal variables H_2 and R_2 and W with time.

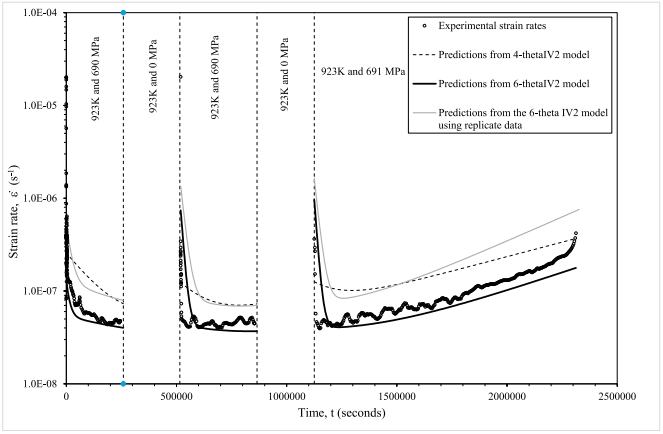

Fig. 12a. Creep strain rates under cyclical unloading (from 690 MPa) at 923K, together with predicted modified strain rates obtained using the 6-θIV2 model with $\lambda = 1$. Solid black line uses the θ values in row 3 of Table 1, whilst the solid grey line uses the θ values in row 2 of Table 1. The dashed line used θ values in row 6 of Table 1.

than H_2 and that its domination of deformation is over early in the test is consistent with this view. It may also be the case that part of H_1, unlike H_2, is fully reversable and so some of the hardening within grain boundaries would then be visco-elastic in nature.

4.3. Cyclical unloading

Fig. 12a plots the creep strain rates obtained during the loaded periods of the unloading test (at 690 MPa and 923K), together with predicted strain rates obtained from the theta values in rows 2 and 3 of Table 1 using the 6-θIV2 model when $\lambda = 1$. The solid black and grey curves show the predicted strain rates obtained using the 6-θIV2 model with $\lambda = 1$. As such these predictions assume softening occurs at the same rates in the loaded and unloaded periods. The difference between these predictions demonstrates just how stochastic creep is, and to get reliable predictions, more than one constant test creep test should be carried out. Taking the solid black curve, it is seen that when the load is applied to the test specimen at the start of the first cycle, there is a very high initial creep rate, that diminishes in magnitude very rapidly. The model overestimates this initial high strain rate when $\lambda = 1$. The model picks up the rapid deceleration of this rate with time but tends to underestimate the actual rate tending as it does to a lower steady state.

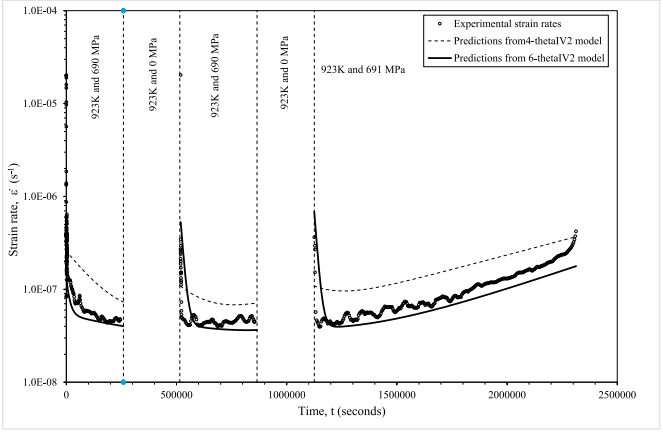

Fig. 12b. Creep strain rates under cyclical unloading (from 690 MPa) at 923K, together with predicted modified strain rates obtained using the 6-θIV2 model with $\lambda = 0.7$. Solid black line uses the θ values in row 3 of Table 1, whilst the dashed line uses the θ values in row 6 of Table 1.

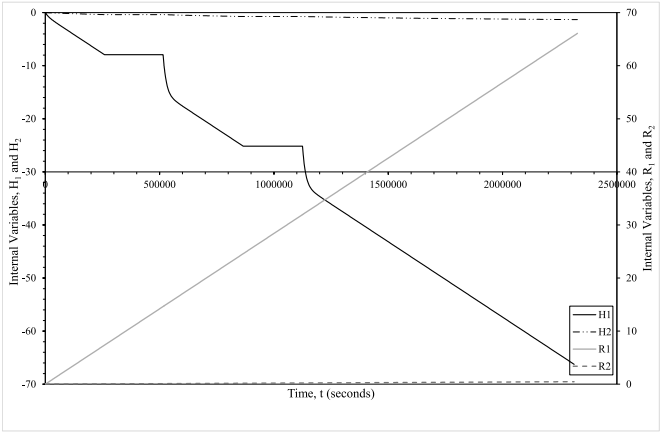

Fig. 13a. Predicted hardening and softening under cyclical unloading (from 690 MPa) at 923K with $\lambda = 1$. All hardening and softening values are based on the θ values in row 3 of Table 1.

When the load is reapplied the model prediction profile is like the first cycle. Halfway through the last cycle the model underestimate the accumulation of damage and thus strain rates. Under the simplifying assumptions stated in the methodology section, the 6-θ model performs much better (than the 4-θ model) at predicting the rapid decline in creep rates at the start of each re-load cycle, it predicts much better the secondary or minimum creep rate and the accumulation of damage in the final cycle.

Fig. 12b plots the predicted strain rates obtained from the theta values in Table 1 using the 6-θIV2 and 4-θIV2 model when $\lambda = 0.7$. The main noticeable difference seen when comparing the predictions in Fig. 12 is that a lower value for λ results in more realistic initial creep rate predictions associated with the start of each cycle. The 6-θ model still performs much better. It also seems reasonable to have a λ value below 1 as softening is likely to occur at a slower rate than that given by $\widehat{R}_1$ and $\widehat{R}_2$ because the stress determines softening rates and this is no present in the unloaded part of the cycle.

Fig. 13a plots the values for the hardening and softening variables over the length of the test. It can be seen that most of the materials hardening is associated with H_1 and the very early stages of primary creep. The assumption of no additional hardening in the unload periods is seen through the horizontal nature of the line during these times. Hardening has a strong non-linear profile with respect to time at the start of each loading cycle but quickly transforms to a linear relationship. The right-hand axis of Fig. 13a plots the two softening variables.

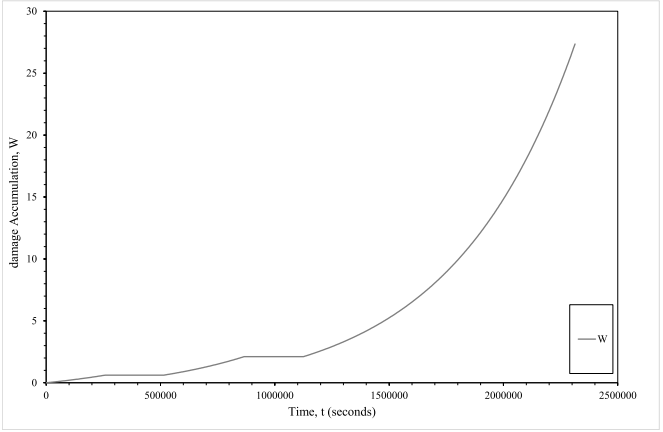

Fig. 13b. Predicted damage accumulation under cyclical unloading (from 690 MPa) at 923K with $\lambda = 1$. Damage values are based on the θ values in row 3 of Table 1.

Again, most of the softening is taking place via mechanisms associated with variable R_1, although recovery of both types continues until the end of test.

Fig. 13b plots the damage variable W. Damage to the material does not take place at a significant level until after around 1,250,000 s of testing when most of the hardening associated with variable H_1 has taken place. Note also the assumption that no damage accumulation occurs during the periods of offloading. Many different interpretations can be placed on these variables that would require further microstructural analysis that would be a valuable source of future research. Some interesting hypotheses that could be studied include the possibility that H_1 represents hardening in the early stages of primary creep with this hardening being confined to grain boundaries within the material and that H_2 then represents hardening taking place within the grains. The fact that H_1 evolves at a faster rate than H_2 and that its domination of deformation is over early on in the test is consistent with this view. It may also be the case that H_1, unlike H_2 is fully reversable and so the hardening within grain boundaries would then be visco-elastic in nature.

5. Conclusions

This paper has developed a theoretical basis for the 6-θ methodology, and showed that when applied to Waspaloy, produces a much better description of primary creep (especially early primary) at constant test conditions. The paper also presented a new internal variable approach for use within this 6-θ methodology to model the accumulation of hardening, softening and damage when specimens are subjected to varying stress and temperature conditions. It was found that this approach produced much better strain rate predictions compared to standard time and strain hardening techniques. It also produced better predictions compared to the implementation of the internal variable approach within the 4-θ methodology. When it came to a simple load-offload test the stochastic nature of creep was clearly apparent with replicate tests producing very different strain rate predictions – illustrating the need to do replicated creep testing to iron out such variability.

Areas for future work include applying these models to other materials and carrying out additional metallographic work to try and relate the measured hardening, softening and damage variables to actual deformation processes within Waspaloy.

CRediT authorship contribution statement

Mark Evans: Writing – review & editing, Writing – original draft, Project administration, Methodology. **Mark Whittaker:** Writing – review & editing, Data curation, Conceptualization. **William Harrison:** Writing – review & editing, Data curation.

Disclosure statement

No potential conflict of interest was reported by the author.

Data statement

The data used in this paper was obtained by Harrison et al. and published in Ref. [1]. Authors have given permission to use this data and to make use of their results and relevant illustrations in this paper.

Declaration of competing interest

No financial or non-financial assistance was provided by a third party for the reported work. This paper was not funded by any research council or any other externalbody.

There are no financial interest or relationship — *within the last 3 years* — related to the subject matter but not directly to this manuscript.

There are no patents or copyrights that are relevant to the work in the manuscript.

There is nothing else of merit to declare.

Appendix

The 6-θ representation of creep can be derived from creep mechanisms in a way similar to that proposed by Evans's [26]. To modify his analysis to account for six θ parameters, the h_α and r_α internal variables discussed in the paper (Equations (7a)-(7c)) need to be split into two sperate groups. h_1 to h_α and r_1 to r_α are hardening and softening variables that occur in the very earliest stages of primary creep, whilst $h_{\alpha+1}$ to h_n and $r_{\alpha+1}$ to r_m are hardening and softening variables that occur after this early primary stage, but before tertiary creep starts

$$\dot{H}_1 = -\widehat{H}_1\dot{\varepsilon}\,; \quad H_1 = \sum_1^{\alpha} h_\alpha \text{ and } \widehat{H}_1 = \sum_1^{\alpha} \widehat{h}_\alpha$$

$$\dot{H}_2 = -\widehat{H}_2\dot{\mu}\,; \quad H_2 = \sum_{\alpha+1}^{n} h_\alpha \text{ and } \widehat{H}_2 = \sum_{\alpha+1}^{n} \widehat{h}_\alpha$$

$$\dot{R}_1 = \widehat{R}_1\,; \quad R_1 = \sum_1^{\alpha} r_\alpha \text{ and } \widehat{R}_1 = \sum_1^{\alpha} \widehat{r}_\alpha \tag{A1}$$

$$\dot{R}_2 = \widehat{R}_2\,; \quad R_2 = \sum_{\alpha+1}^{m} r_\alpha \text{ and } \widehat{R}_2 = \sum_{\alpha+1}^{m} \widehat{r}_\alpha$$

where $\dot{\mu}$ is the creep rate occurring after very early primary creep. Damage proceeds as before

$$\dot{W} = \widehat{W}\dot{\varepsilon}_T\,; \quad W = \sum_{\alpha=1}^{p} w_\alpha \text{ and } \widehat{W} = \sum_{\alpha=1}^{p} \widehat{w}_\alpha$$

where $\dot{\varepsilon}_T$ is the tertiary creep rate. This then allows the creep constitutive law of Equation (7d) to be written as

$$\dot{\varepsilon} = \dot{\varepsilon}_o(1 + H_1 + H_2 + R_1 + R_2 + W) \tag{A2}$$

At constant stress and temperature, $\widehat{H}_1, \widehat{R}_1, \widehat{H}_2, \widehat{R}_2$ and $\widehat{W}$ are also constant, and if $H_1 = R_1 = H_2 = R_2 = W = 0$, when $t = 0$, then the differential of Equation (A2) with respect to time is

$$\ddot{\varepsilon} = \dot{\varepsilon}_o(\dot{H}_1 + \dot{R}_1) = \dot{\varepsilon}_o(\widehat{R}_1 - \widehat{H}_1\dot{\varepsilon}) \tag{A3}$$

for very small times in relation to creep life, i.e. where the effects of H_2, R_2 and W are negligible (namely very early primary creep). Upon integration

$$\int_{\dot{\varepsilon}_o}^{\dot{\varepsilon}} \frac{1}{((\widehat{R}_1 - \widehat{H}_1\dot{\varepsilon}))} d\dot{\varepsilon} = \dot{\varepsilon}_o \int_0^t dt$$

$$\ln[(\widehat{R}_1 - \widehat{H}_1\dot{\varepsilon})] + C = -\widehat{H}_1\dot{\varepsilon}_o t \tag{A4}$$

where C is the constant of integration. When $t = 0$, $\dot{\varepsilon} = \dot{\varepsilon}_o$ and so $C = -\ln((\widehat{R}_1 - \widehat{H}_1\dot{\varepsilon}_o)$. Thus

$$\ln\left[\frac{(\widehat{R}_1 - \widehat{H}_1\dot{\varepsilon})}{(\widehat{R}_1 - \widehat{H}_1\dot{\varepsilon}_o)}\right] = -\widehat{H}_1\dot{\varepsilon}_o t$$

Then rearranging for $\dot{\varepsilon}$

$$\dot{\varepsilon} = \left[\dot{\varepsilon}_o - \frac{\widehat{R}_1}{\widehat{H}_1}\right] e^{-\widehat{H}_1\dot{\varepsilon}_o t} + \frac{\widehat{R}_1}{\widehat{H}_1} \tag{A5}$$

Equation (A5) states that an initial very high creep rate of $\dot{\varepsilon}_o$, gives way to a rapidly decreasing creep rate until a steady state rate of creep is reached, i.e. the rate $\frac{\widehat{R}_1}{\widehat{H}_1}$ is reached. The value for this steady state creep rate is determined by the rate of work hardening $\widehat{H}_1$ in relation to the rate of softening, $\widehat{R}_1$ occurring during very early primary creep. This is a very general specification to which a variety of different creep mechanisms can be attached to it. For example, H_1 and R_1 may represent creep processes confined to grain boundaries. Then the hardening and recovery processes associated with H_2 and R_2 could represent processes occurring within the grains. It's possible that H_2 and R_2 are also active during this very early primary creep, but the above representation implies the effect of this on total strain will be negligible and unable to prevent the tendency towards this steady state during very early creep. However, as time progresses, other creep processes will start to dominate the determination of overall strain. This can be modelled by assuming that the hardening and recovery processes occurring after very early primary creep influence the value for $\dot{\rho}_{1o} = \frac{\widehat{R}_1}{\widehat{H}_1}$

$$\dot{\varepsilon} = \left[\dot{\varepsilon}_o - \frac{\widehat{R}_1}{\widehat{H}_1}\right] e^{-\widehat{H}_1\dot{\varepsilon}_o t} + \frac{\widehat{R}_1}{\widehat{H}_1}[1 + H_2 + R_2] \tag{A6}$$

Extracting the early primary creep strain rates

$$\dot{\mu} = \dot{\varepsilon} - \left[\dot{\varepsilon}_o - \frac{\widehat{R}_1}{\widehat{H}_1}\right] e^{-\widehat{H}_1\dot{\varepsilon}_o t} \tag{A7}$$

with $\dot{\mu} = \frac{\widehat{R}_1}{\widehat{H}_1}[1 + H_2 + R_2]$ representing latter primary creep. Upon differentiation

$$\ddot{\mu} = \frac{\widehat{R}_1}{\widehat{H}_1}[\dot{H}_2 + \dot{R}_2] = \frac{\widehat{R}_1}{\widehat{H}_1}(\widehat{R}_2 - \widehat{H}_2\dot{\mu}) \tag{A8}$$

which upon integration

$$\int_{\dot{\rho}_{1o}}^{\dot{\mu}} \frac{1}{((\widehat{R}_2 - \widehat{H}_2\dot{\mu}))} d\dot{\mu} = \dot{\rho}_{1o} \int dt$$

gives

$$\dot{\mu} = \left[\dot{\rho}_{1o} - \frac{\widehat{R}_2}{\widehat{H}_2}\right] e^{-\widehat{H}_2\dot{\rho}_{1o} t} + \frac{\widehat{R}_2}{\widehat{H}_2} \tag{A9}$$

Then, using Equation (A7)

$$\dot{\varepsilon} = \left[\dot{\varepsilon}_o - \frac{\widehat{R}_1}{\widehat{H}_1}\right] e^{-\widehat{H}_1\dot{\varepsilon}_o t} + \dot{\mu} = \left[\dot{\varepsilon}_o - \frac{\widehat{R}_1}{\widehat{H}_1}\right] e^{-\widehat{H}_1\dot{\varepsilon}_o t} + \left[\dot{\rho}_{1o} - \frac{\widehat{R}_2}{\widehat{H}_2}\right] e^{-\widehat{H}_2\dot{\rho}_{1o} t} + \frac{\widehat{R}_2}{\widehat{H}_2} \tag{A10}$$

Equation (A10) states that as primary creep comes to an end, the creep rate approaches a value of $\frac{\widehat{R}_2}{\widehat{H}_2}$. But even when damage (the formation of intergranular cavities and nucleation of cracks) occurs during primary creep, this damage will be small and unable to prevent the rapid decay in the primary creep rate towards the minimum rate $\dot{\varepsilon}_m$. However, as damage progresses with increasing strain, the creep rate will start to accelerate, and this

will offset the gradual decay of the creep rate towards $\dot{\varepsilon}_m = \frac{\widehat{R}_2}{\widehat{H}_2}$. Damage W influences the minimum creep rate $\dot{\varepsilon}_m = \frac{\widehat{R}_2}{\widehat{H}_2}$

$$\dot{\varepsilon} = \left[\dot{\varepsilon}_o - \frac{\widehat{R}_1}{\widehat{H}_1}\right] e^{-\hat{H}_1 \dot{\varepsilon}_o t} + \left[\dot{\rho_{1o}} - \frac{\widehat{R}_2}{\widehat{H}_2}\right] e^{-\hat{H}_2 \dot{\rho_{1o}} t} + \frac{\widehat{R}_2}{\widehat{H}_2}[1 + W] \tag{A11}$$

or, upon extracting all primary creep

$$\dot{\varepsilon}_T = \frac{\widehat{R}_2}{\widehat{H}_2}[1 + W] \tag{A12}$$

where $\dot{\varepsilon}_T$ is the tertiary strain rate. Upon differentiation

$$\ddot{\varepsilon}_T = \frac{\widehat{R}_2}{\widehat{H}_2}[\dot{W}] = \frac{\widehat{R}_2}{\widehat{H}_2}\widehat{W}\dot{\varepsilon}_T$$

and subsequent integration

$$\int_{\dot{\varepsilon}_m}^{\dot{\varepsilon}_T} \frac{1}{\dot{\varepsilon}_m \dot{\varepsilon}_T} d\dot{\varepsilon}_T = \widehat{W} \int dt \tag{A13}$$

or

$$\ln\left[\frac{\dot{\varepsilon}_T}{\dot{\varepsilon}_m}\right] = \frac{\widehat{R}_2}{\widehat{H}_2}\widehat{W}t$$

Solving for $\dot{\varepsilon}_T$ gives

$$\dot{\varepsilon}_T = \frac{\widehat{R}_2}{\widehat{H}_2} e^{\frac{\hat{R}_2}{\hat{H}_2}\hat{W}t} \tag{A14}$$

Substituting this into Equation (A11)gives

$$\dot{\varepsilon} = \left[\dot{\varepsilon}_o - \frac{\widehat{R}_1}{\widehat{H}_1}\right] e^{-\hat{H}_1 \dot{\varepsilon}_o t} + \left[\dot{\rho_{1o}} - \frac{\widehat{R}_2}{\widehat{H}_2}\right] e^{-\hat{H}_2 \dot{\rho_{1o}} t} + \frac{\widehat{R}_2}{\widehat{H}_2} e^{\frac{\hat{W}\hat{R}_2}{\hat{H}_2}t} \tag{A15}$$

This states that when there is no damage occurring, the creep rate tends to $\frac{\widehat{R}_2}{\widehat{H}_2}$. Then as strain accumulates over time this minimum creep rate is accelerated by the factor $e^{\frac{\hat{W}\hat{R}_2}{\hat{H}_2}t}$ which represents damage accumulation. This does not mean that damage does not develop during the time that primary creep occurs, but only that the effect of that part of the primary strain due to decaying rates is small.

Data availability

Data will be made available on request.

References

[1] K. Sawada, K. Kimura, F. Abe, Y. Taniuchi, K. Sekido, T. Nojima, Catalog of NIMS creep data sheets, Sci. Technol. Adv. Mater. 20 (1) (2019) 1131–1149.
[2] S. Holdsworth, The european creep collaborative committee (ECCC) approach to creep data assessment, J. Pressure Vessel Technol. 130 (2) (2008) 024001 (6 pages).
[3] BSCC High Temperature Data, British Long Term Creep Rupture and Elevated Temperature Tensile Data on Steels for High Temperature Service Volume 156 of, ISI publication, 1974, p. 725. ISSN 0536-2016.
[4] W.J. Harrison, M.T. Whittaker, C. Deen, Creep behaviour of waspaloy under non-constant stress and temperature, Mater. Res. Innov. 17 (5) (2013) 323–326.
[5] R.W. Evans, B. Wilshire, Creep of Metals and Alloys, Institute of Metals, London, Appendix, 1985.
[6] M.T. Whittaker, W.J. Harrison, C. Deen, C. Rae, S. Williams S, Creep deformation by dislocation movement in waspaloy, Materials 10 (61) (2017) 1–14.
[7] J. Parkin, S. Birosca, Crystallographic orientation influence on slip system activation and deformation mechanisms in waspaloy during in-situ mechanical loading, J. Alloys Compd. 865 (5) (2021) 158548.
[8] A. Graham, K.F.A. Walles, Relations between long- and short-time properties of commercial alloys, JISI 193 (1995) 105.
[9] G. McVetty, Factors Affecting the Choice of Working Stresses for High Temperature Service Transactions ASME, 1933, p. 99, 55.
[10] F. Phillips, The slow stretch in India rubber, glass and metal wire when subjected to a constant pull, Philos. Mag. 9 (1905) 513.
[11] D. McHenry, A new aspect of creep in concrete and its application to design, Proc. ASTM 43 (1943) 1069.
[12] Y.N. Rabotnov, Creep Problems in Structural Members, North-Holland, Amsterdam, 1969.
[13] M. Kachanov, Izv Akad Navk SSR, vol. 8, 1958, p. 26.
[14] R. Sandström, A. Kondyr, A model for tertiary creep in Mo- and CrMo-steels, in: Proceedings of Third International Conference on Mechanical Behaviour of Materials, Cambridge, 1979.
[15] F.N. Norton, The Creep of Steel at High Temperature, McGraw-Hill, New York, 1929.
[16] A.M. Othman, D.R. Hayhurst, Multi-axial creep rupture of a model structure using a two-parameter material model, Int. J. Mech. Sci. 32 (1) (1990) 35–48.
[17] K. Maruyama, J. Nakamura, K. Yoshimi, Y. Nagae, Evaluation of long-term creep rupture life of gr. 91 steel by analysis of on-going creep curves. Advances in Materials Technology for Fossil Power Plants Proceedings from the Eighth International Conference October 11–14, 2016. Albufeira, Algarve, Portugal.
[18] X. Wu, S. Williams, D. Gong, A true-stress creep model based on deformation mechanisms for polycrystalline materials, J. Mater. Eng. Perform. 21 (2012) 2255–2262.
[19] S.R. Holdsworth, M. Askins, A. Baker, E. Gariboldi, S. Holmstrom, A. Klenk, M. Ringel, G. Merckling, R. Sandstrom, M. Schwienheer, S. Spigarelli, Factors influencing creep model equation selection, International Journal of Pressure Vessels 85 (1–2) (2008) 80–88.
[20] H. Liu, F. Peng, Y. Zhang, Y. Li, K. An, Y. Yang, Y. Zhang, X. Guan, W. Zhu, A new modified theta projection model for creep property at high temperature, J. Mater. Eng. Perform. 29 (2020) 4779–4785.
[21] S. Moon, J.-M. Kim, J.-Y. Kwon, B.-S. Lee, K.-J. Choi, M.-C. Kim, S. Han, Modified θ projection model-based constant-8stress creep curve for alloy 690 steam generator tube material, Nucl. Eng. Technol. 54 (3) (2022) 917–925.
[22] W. Harrison, Z. Abdallah, M. Whittaker, A model for creep and creep damage in the γ-titanium aluminide Ti-45Al-2Mn-2Nb, Materials 17 (3) (2014) 2194–2209.

[23] Y. Zheng, S. Yang, X. Ling, Creep life prediction of small punch creep testing specimens for service-exposed Cr5Mo using the theta-projection method, Eng. Fail. Anal. 72 (2017) 58–66.
[24] R.W. Evans, The θ projection method and low creep ductility materials, Mater. Sci. Technol. 16 (2000) 6–8.
[25] R.W. Evans, P.J. Scharning, The θ projection method applied to small strain creep of a commercial Al alloy, Mater. Sci. Technol. 1 (5) (2001) 487–493.
[26] R.W. Evans, A constitutive model for the high-temperature creep of particle-hardened alloys based on the Θ projection method, Royal Society Proceedings: Math. Phys. Eng. Sci. 456 (1996) 835–868, 2000.
[27] F.C. Monkman, N.J. Grant, An empirical relationship between rupture life and minimum creep rate in creep-rupture tests, Proc. Am. Soc. Test. Mater. 56 (1956) 593–620.
[28] R.W. Evans, Statistical scatter and variability of creep property estimates in θ projection method, Mater. Sci. Technol. 5 (7) (1989) 699–707.